The Representation of Speech in a Biophysically Detailed Model of the Ventral Cochlear Nucleus

Melih Yayli, Ian C. Bruce

Department of Electrical & Computer Engineering, McMaster University, Hamilton, ON, Canada

Abstract

Biophysically detailed representations of neural network models provide substantial insight to underlying neural processing mechanisms in auditory systems. For simple biological systems the behavior can be represented by simple equations or flow charts. But for complex systems more detailed descriptions of individual neurons and their synaptic connectivity are typically required. Creating extensive network models allows us to test hypotheses, apply specific manipulations that cannot be done experimentally and provide supporting evidence for experimental results. Several studies have been made on establishing realistic models of the cochlear nucleus (Eager et al., 2004; Manis and Campagnola, 2018), the part of the brainstem where sound signals enter the brain, both on individual neuron and networked structure levels. These models are based on both in vitro and in vivo physiological data, and the models successfully demonstrate certain aspects of the neural processing of sound signals. Even though these models have been tested by using tone bursts and isolated phonemes as stimuli, the representation of speech in the cochlear nucleus and how it may support robust speech intelligibility remains to be explored with these detailed biophysical models. In this study, a biophysically detailed model of microcircuits in the cochlear nucleus is created based on Manis and Campagnola (2018). We have updated this model to take inputs from the new phenomenological auditory periphery model of Bruce et al. (2018). Different cell types in the cochlear nucleus are modelled by detailed cell models of Rothman and Manis (2003). Networked structures are built out of them according to published anatomical and physiological data. The outputs of these networked structures are used to create neurograms to investigate the representation of different phonemes and words and are compared to published physiological data (Blackburn and Sachs, 1990; Delgutte et al., 1998). The ultimate goal of this study is to incorporate physiologically-detailed models of brainstem processing into neural-based predictors of speech intelligibility.

I. INTRODUCTION

- The cochlear nucleus (CN) is the first stage where auditory information enters the brain. Auditory nerve fibers project to the different areas of the cochlear nucleus such that the tonotopic organization is preserved (Fig. 1).

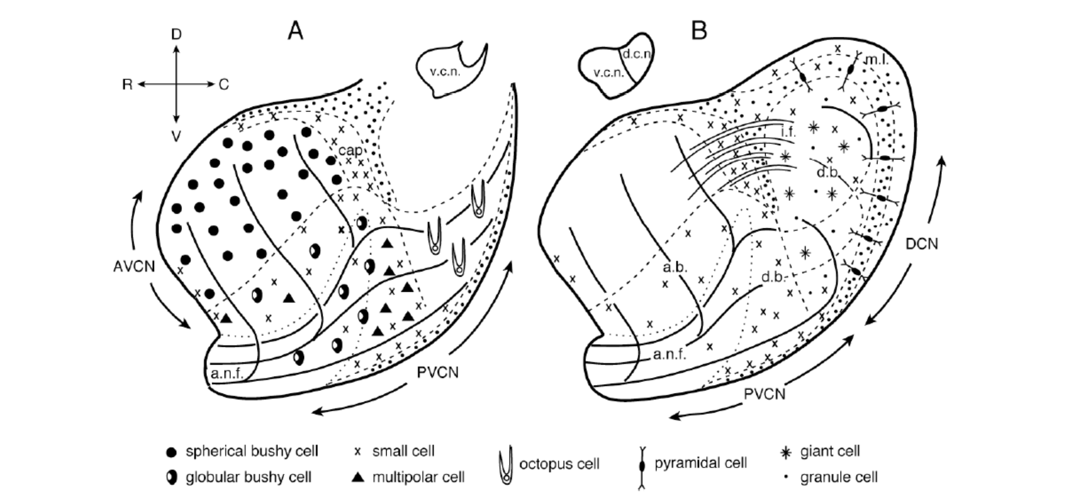

Figure 1: The sagittal view of the cochlear nucleus and the distribution of cell types. Abbreviations: posteroventral cochlear nucleus (PVCN), anteroventral cochlear nucleus (AVCN), dorsal cochlear nucleus (DCN), ventral cochlear nucleus (VCN). From Young and Oertel (2004)

- Auditory nerve (AN) fibers have similar physiological properties, therefore modeling their behavior as a population can be achieved by adding small variations the one type of model. In contrast, the cochlear nucleus has several different type of cells which show different behaviors. This diversity makes the cochlear nucleus an important feature extractor. Each cell type selectively emphasizes different aspects of the sound signal to form sound localization, temporal fluctuations and frequency spectrum cues.
- Multiple parallel pathways of the CN using different cell types is an advantage. The distinction between the functions of these parallel pathways (i.e. sound identification and sound localization cues) becomes less prominent as features reach to the upper levels of central auditory system since the features are combined and get more complex in structure. This motivates accurate modeling of the CN neural circuitry, to faithfully capture how it processes the information it receives from the AN and extracts sound features that are used in higher brain centers.

II. MODEL STRUCTURE AND COMPUTATIONAL IMPLEMENTATION

- The phenomenological AN model of Bruce et al. (2018) provides inputs to the VCN cell models.

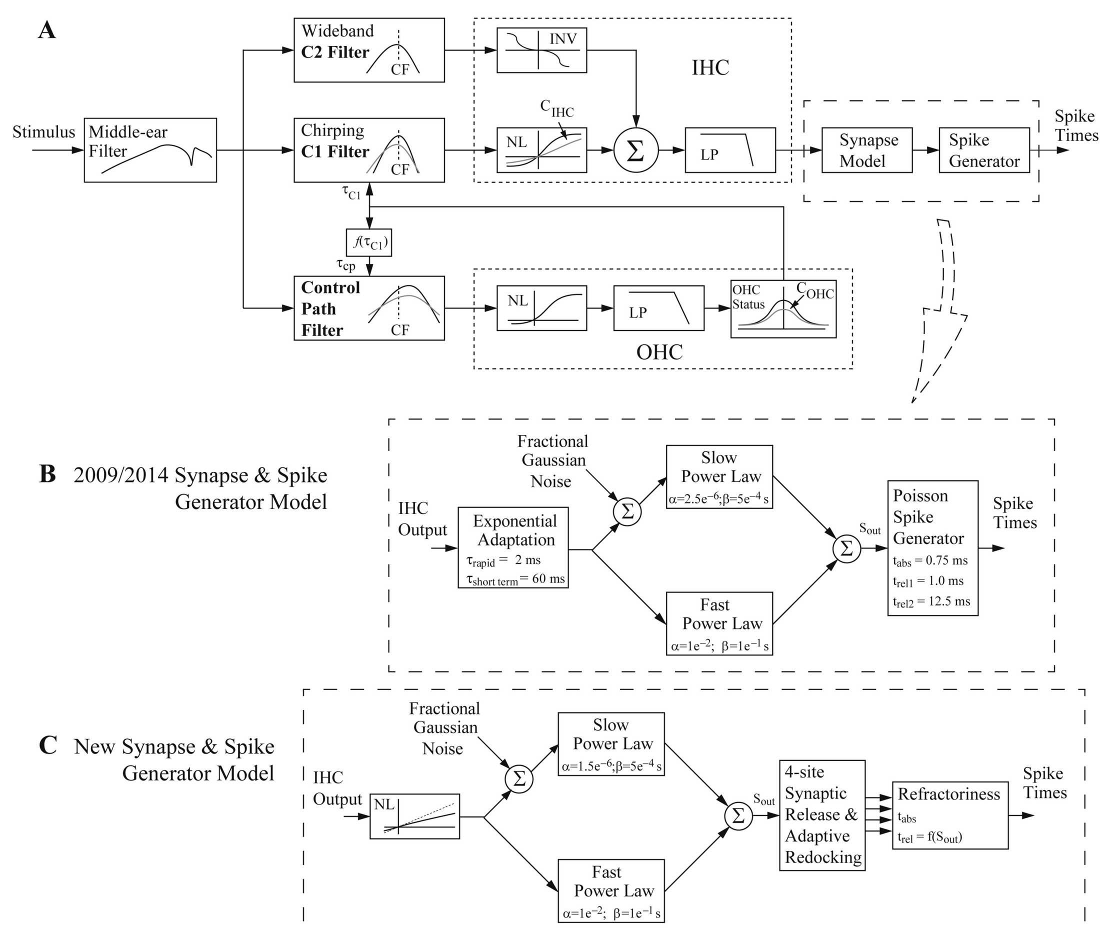

Figure 2: Bruce et al. (2018) auditory periphery model. Panel B and C compares the old model with the new one. The new model has updated synapse and spike generator. Abbreviations: outer hair cell (OHC), inner hair cell (IHC), low-pass (LP) filter, static nonlinearity (NL), characteristic frequency (CF), and inverting nonlinearity (INV). From Bruce et al. (2018).

- Rothman and Manis (2003) type VCN cell models are used at first to test model mechanisms.
- The exp2syn function created for this research is based on Carnevale and Hines (2006) exp2syn function from NEURON. Cell connections are modelled as simple exponential decay with a time constant of 0.4 msec for excitatory connections and double exponential function with time constants of 0.4 msec and 2.5 msec for inhibitory connections.
- Individual cell models are tested by applying current injections. The results are compared with Rothman and Manis (2003). Next, small microcircuits are formed and tested by applying tone bursts.
- The synaptic convergence (multiple presynaptic cells connected to one postsynaptic cell) is modelled as follows: presynaptic cell output voltages are translated to spike trains, corresponding spike trains for excitatory and synaptic inputs are added together, each spike's effect on postsynaptic cell modelled as an exponential change in the synaptic conductance. The resulting current is added to the membrane voltage equation as a synaptic channel input. Apart from the synaptic input channel I_s which consists of excitatory and inhibitory synaptic inputs, the model used in this study also includes a fast inactivating Na^+ current (I_{Na^+}), a hyperpolarization activated cation current (I_h), a leakage current (I_{leak}), and I_{ext} to simulate the injected current mechanism. The change in the membrane voltage is calculated as:

$$C_m \frac{dV}{dt} = -(I_{HT} + I_{LT} + I_A + I_h + I_{lk} + I_s - I_{ext}) \quad (1)$$

- The network structure and parameters are based on Manis and Campagnola's modeling platform for VCN microcircuits. Manis and Campagnola (2018) used modified Rothman and Manis (2003) cell models according to their recent works (Campagnola and Manis, 2014; Xie and Manis, 2013, 2017). For input they used the older auditory periphery model of Zilany et al. (2014, 2009).

Table 1: Synaptic Convergence Parameters (number of cells)

	Model Type					
	bushy	tstellate	dstellate	octopus	pyramidal	tuberculoventral
ANF	3.3	6.5	35	60	48	24
dstellate	7	20	3	0	15	15
tstellate	0	0	0	0	0	0
tuberculoventral	6	6	0	0	21	0
pyramidal	0	0	0	0	0	0

Table 2: Synaptic Convergence Range Parameters (octaves)

	Model Type					
	bushy	tstellate	dstellate	octopus	pyramidal	tuberculoventral
ANF	0.05	0.1	0.4	0.5	0.1	0.1
dstellate	0.208	0.347	0.5	0	0.2	0.2
tstellate	0.1	0.1	0	0	0	0
tuberculoventral	0.069	0.111	0	0	0.15	0
pyramidal	0	0	0	0	0	0

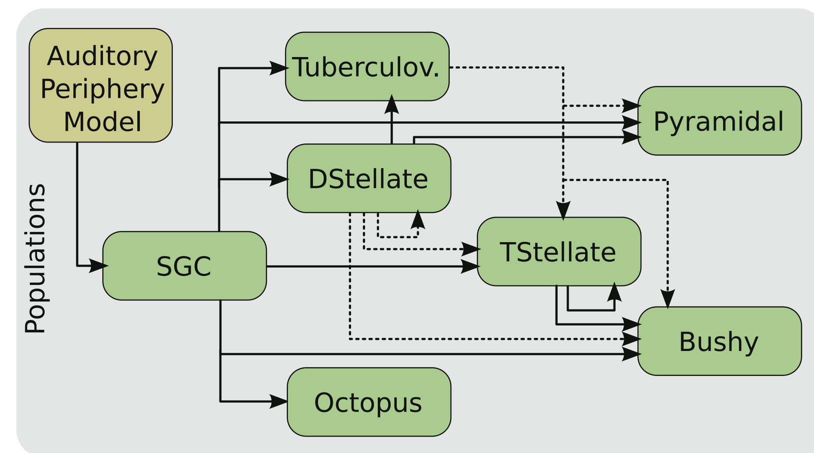

Figure 3: Manis and Campagnola (2018) model of the VCN. Solid lines indicate excitatory connections while dashed lines are inhibitory. The model takes channel equations from NEURON and create cells in a Python environment. Parameters used in this system to create cells and specific connectivity parameters can be found in the repository; `http://www.github.com/cnmodel`. From Manis and Campagnola (2018).

III. RESULTS

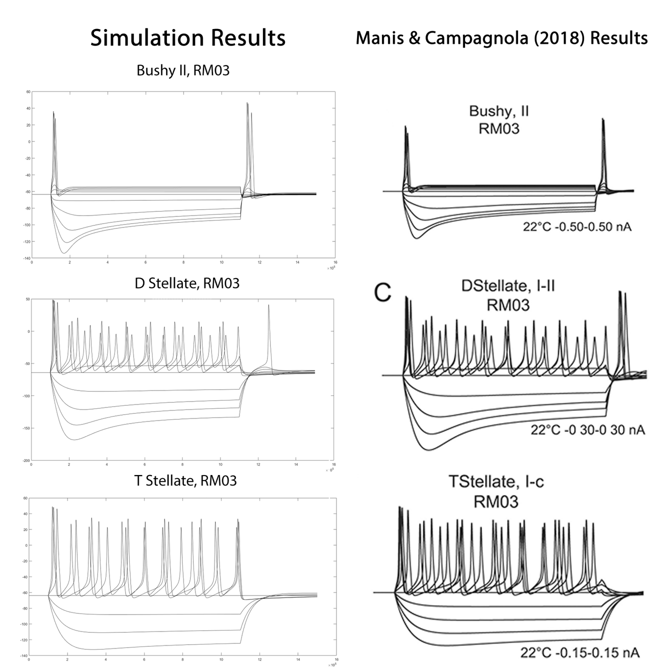

Figure 4: Comparison of current injection simulation results with cell model results presented in Manis and Campagnola (2018).

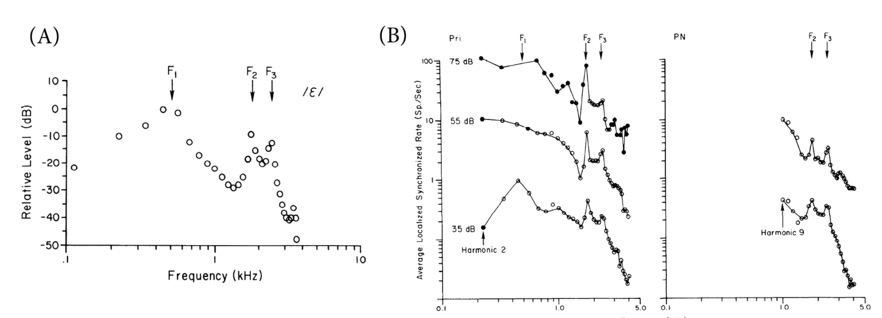

Figure 5: (A) Frequency spectrum representation of vowel /ε/. The arrows show the formant frequencies: F1 = 512 Hz, F2 = 1.792 kHz, F3 = 2.432 kHz. From Blackburn and Sachs (1990) (B) Recorded ALSR responses of Pri (left panel) and PriN (right panel) units to vowel /ε/. From Blackburn and Sachs (1990).

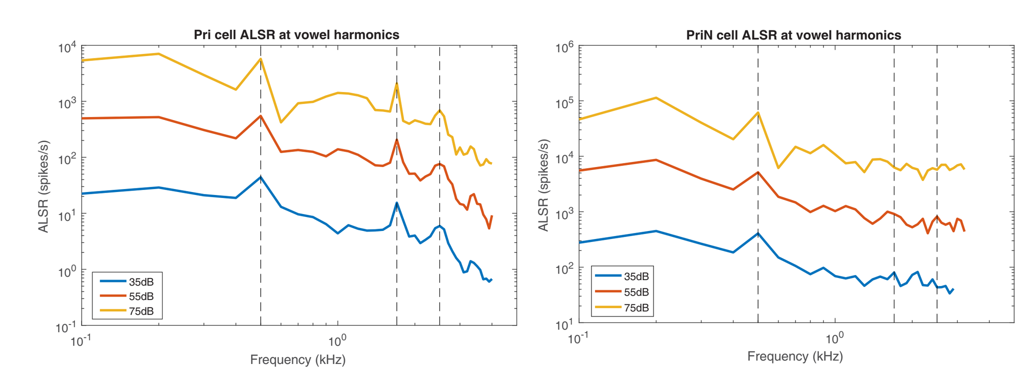

Figure 6: Comparison of ALSR simulation results of Pri (spherical bushy) and PriN (globular bushy) cells for different input sound pressure levels.

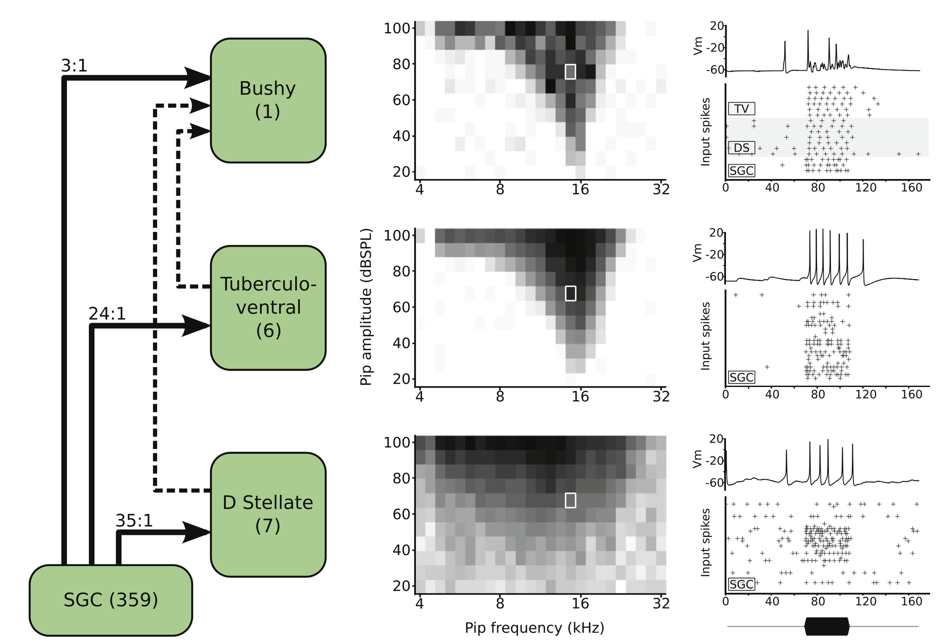

Figure 7: A microcircuit created with the Manis and Campagnola (2018) modeling platform. The first layer consists of 7 DS cells that take input from 35 AN fibers with various spont rates (SRs). The second layer has 6 TV cells taking excitatory inputs from 24 AN fibers with low and medium SRs. The inhibitory input from DS to TV is disregarded for this simulation. The output bushy cell receives 3 excitatory AN inputs and receives inhibitory inputs from TV and DS cells. The middle column shows the response maps of cells to different frequency and amplitude tone stimuli. The third column shows the cells' spiking behavior for a 76 dB SPL, $\sim$15 kHz tone pip. From Manis and Campagnola (2018).

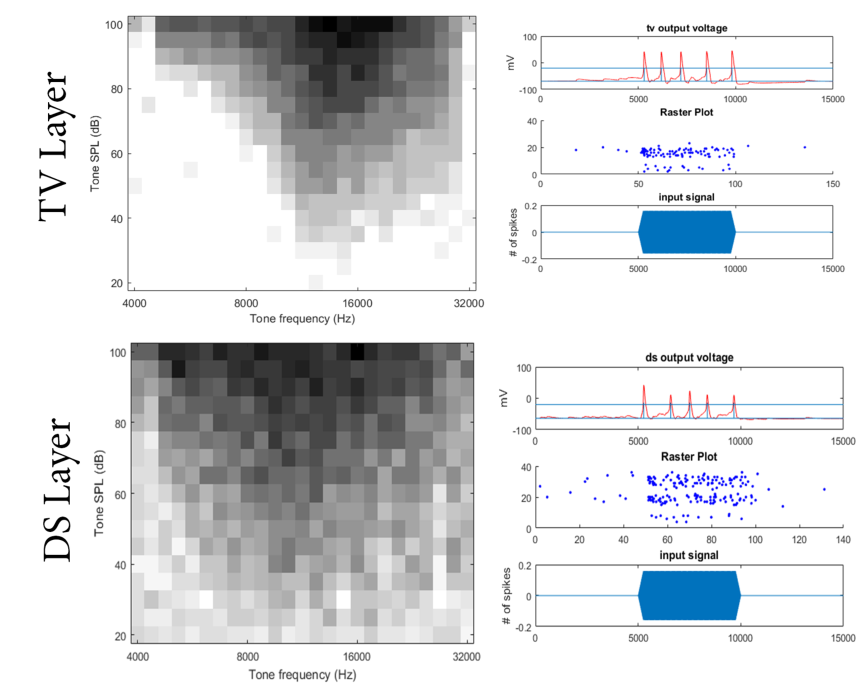

Figure 8: The left column shows Manis and Campagnola (2018) type DS and TV cell response maps. The right column shows an iteration of the simulation when the tone intensity is 75 dB and the frequency is $\sim$15 kHz. The top panel shows the membrane voltage of cells and spike trains created from them. The middle panel shows the raster plot of AN inputs. The bottom panel shows the input tone pip.

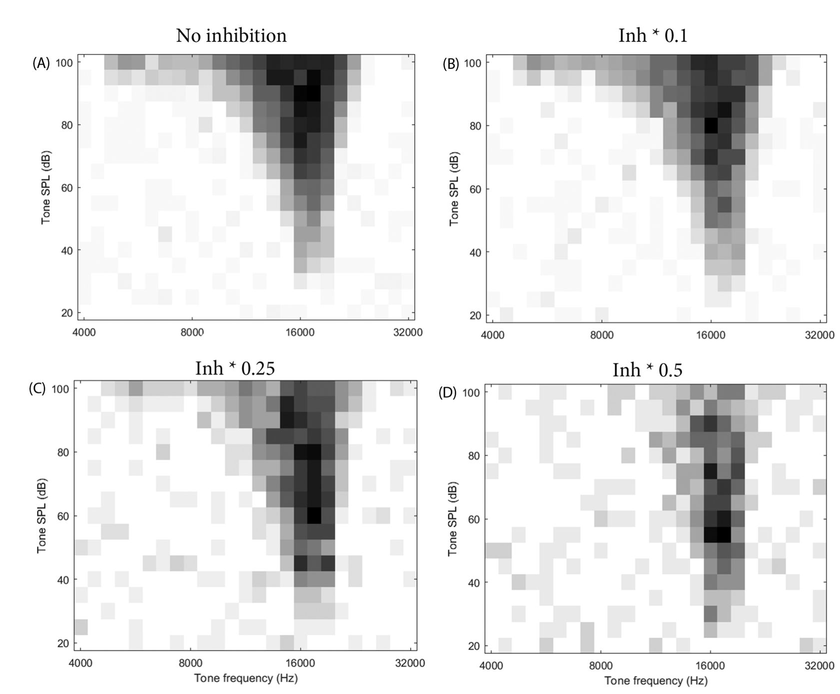

Figure 9: Manis and Campagnola (2018) type bushy cell response maps for different inhibitory input configurations. (A) No inhibition, 3 suprathreshold AN inputs are applied. (B) With inhibition from DS and TV cells multiplied by 0.1. (C) The inhibitory multiplier raised to 0.25. (D) The inhibitory multiplier raised to 0.5.

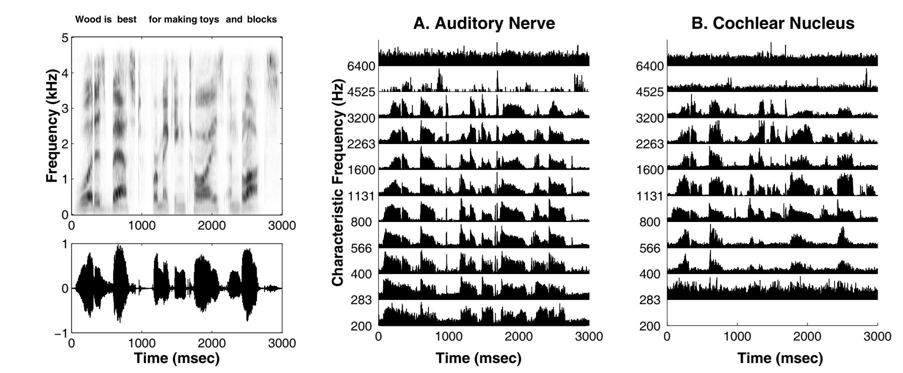

Figure 10: Delgutte et al. (1998) recordings taken from AN and CN cell populations stimulated with a sentence: 'Wood is best for making toys and blocks'. The CN cell population consisted almost entirely of primary-like, chopper and pauser neurons.

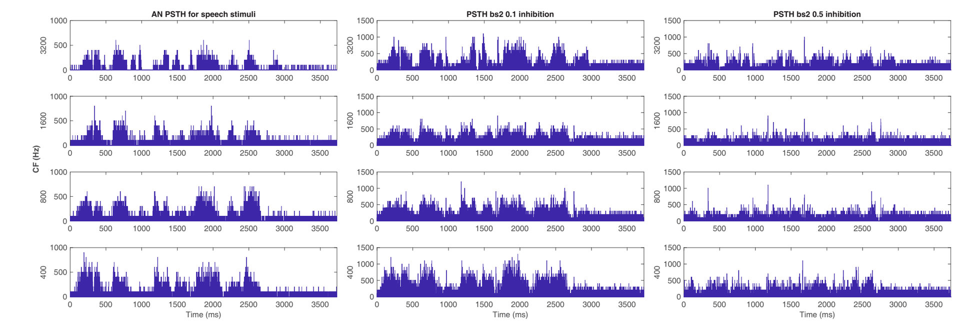

Figure 11: Different CF model AN (left-hand panel) and bushy cell microcircuit (middle and right-hand panels) responses to the sentence used in Delgutte et al. (1998). The effect of the strength of inhibition on the CN firing patterns can be seen between the middle (inhibitory multiplier = 0.1) and right-hand (inhibitory multiplier = 0.5) panels.

IV. CONCLUSIONS

- Manis and Campagnola (2018) tested their new model through the same general procedures as Rothman and Manis (2003). However, only a subset of simulation results were presented in Manis and Campagnola (2018), and they did not perform an extensive testing of the strength of inhibitory inputs in their model. Therefore the results obtained in our study could not be compared directly with simulation results from other research. However, by taking physiological data and Rothman and Manis (2003) cell model responses into consideration, the updated Manis and Campagnola (2018) cell models developed in this study are seen to have close resemblance to the real world data.
- Inhibition effects on firing behavior of cells were inspected by creating a bushy cell microcircuit. In this microcircuit, inhibition was produced by DS and TV cells. The results show that inhibitory inputs have a large effect in regulating the firing behavior of the main cell types of the VCN. As the inhibitory inputs become stronger, the tuning of bushy cell responses to excitatory ANF inputs becomes sharper.
- To create PSTH plots, 100 or 500 iterations are used. ALSR plots require simulation of ANFs with a large range of CFs and spont rates. Therefore, simulations to create these plots need a huge amount of time and computational power. One possible solution is parallelizing the code and using a high-performance computing system for submitting jobs with different parameter sets. This will allow us to explore the effects of different configurations of inhibitory inputs on microcircuit responses. Future work will also expand the focus to include other VCN cell types, particular those with chopper responses.

REFERENCES

Blackburn, C. C. and Sachs, M. B. (1990). The representations of the steady-state vowel sound/e/in the discharge patterns of cat anteroventral cochlear nucleus neurons. *Journal of neurophysiology*, 63(5):1191–1212.

Bruce, I. C., Erfani, Y., and Zilany, M. S. (2018). A phenomenological model of the synapse between the inner hair cell and auditory nerve: Implications of limited neurotransmitter release sites. *Hearing research*, 360:40–54.

Campagnola, L. and Manis, P. B. (2014). A map of functional synaptic connectivity in the mouse anteroventral cochlear nucleus. *Journal of Neuroscience*, 34(6):2214–2230.

Carnevale, N. T. and Hines, M. L. (2006). *The NEURON book*. Cambridge University Press.

Delgutte, B., Hammond, B., and Cariani, P. (1998). Neural coding of the temporal envelope of speech: relation to modulation transfer functions. *Psychophysical and physiological advances in hearing*, pages 595–603.

Eager, M. A., Grayden, D. B., Burkitt, A. N., and Meffin, H. (2004). A neural circuit model of the ventral cochlear nucleus. In *Proc 10th Aust Int Conf on Speech Science & Technology, SST*, pages 539–544.

Manis, P. B. and Campagnola, L. (2018). A biophysical modelling platform of the cochlear nucleus and other auditory circuits: from channels to networks. *Hearing research*, 360:76–91.

Rothman, J. S. and Manis, P. B. (2003). The roles potassium currents play in regulating the electrical activity of ventral cochlear nucleus neurons. *Journal of neurophysiology*, 89(6):3097–3113.

Xie, R. and Manis, P. B. (2013). Target-specific ipsc kinetics promote temporal processing in auditory parallel pathways. *Journal of Neuroscience*, 33(4):1598–1614.

Xie, R. and Manis, P. B. (2017). Radiate and planar multipolar neurons of the mouse anteroventral cochlear nucleus: Intrinsic excitability and characterization of their auditory nerve input. *Frontiers in neural circuits*, 11:77.

Zilany, M. S., Bruce, I. C., and Carney, L. H. (2014). Updated parameters and expanded simulation options for a model of the auditory periphery. *The Journal of the Acoustical Society of America*, 135(1):283–286.

Zilany, M. S., Bruce, I. C., Nelson, P. C., and Carney, L. H. (2009). A phenomenological model of the synapse between the inner hair cell and auditory nerve: long-term adaptation with power-law dynamics. *The Journal of the Acoustical Society of America*, 126(5):2390–2412.

yaylim@mcmaster.ca |ibruce@ieee.org

Supported by NSERC (Discovery Grant No. 261736), and the Turkish Ministry of Education